JOURNAL OF GEOPHYSICAL RESEARCH, VOL. 111, B08402, doi:10.1029/2005JB003882, 2006

Click Here for Full Article

Patterns of stress and strain rate in southern Africa

Peter Bird,[1] Zvi Ben-Avraham,[2,3] Gerald Schubert,[1,4] Marco Andreoli,[5,6] and Giulio Viola[7]

Received 10 June 2005; revised 15 February 2006; accepted 2 March 2006; published 11 August 2006.

[1] The southward propagation of the East Africa rift presents an opportunity to study plate boundary formation. We tabulate orientation data which confirm the province of NW-SE directed most compressive horizontal principal stress (''Wegener stress anomaly'') earlier tentatively attributed to ridge push. We also collect information on stress ''regime,'' described by the associated Andersonian fault type(s). We use thin shell finite element models with realistic rheology to test three causes of stress: (1) lateral variations in density moment, (2) resistance of unbroken lithosphere to relative plate rotation, and (3) stress concentration ahead of a crack tip. Models with stress due primarily to variations in density moment are unsuccessful in their predictions (59–73% incorrect regimes; 32–40° azimuth errors). Models in which Africa-Somalia spreading is regulated at realistic rates by remote boundary conditions are more accurate (18–41% incorrect regimes; 25–35° azimuth errors). Treating the East Africa rift as a frictionless crack degrades the fit in either case. Apparently, the Wegener stress anomaly is caused primarily by resistance to the relative rotation between the Somalia and Africa plates. The East Africa rift north of 21°S may be weakened by strain but has residual friction $\geq$0.1. Greater strength of oceanic lithosphere is likely to cause stress increases, reorientations, and regime changes offshore. The predicted strain rate map has high rates along the rift, curving at 12°S into a western arc through Angola-Namibia-South Africa. Seismic hazard in Namibia may be greater than the instrumental catalog suggests. However, a number of unfit data indicate that these models represent only a first step.

Citation: Bird, P., Z. Ben-Avraham, G. Schubert, M. Andreoli, and G. Viola (2006), Patterns of stress and strain rate in southern Africa, *J. Geophys. Res.*, *111*, B08402, doi:10.1029/2005JB003882.

1. Introduction

[2] Most studies of neotectonics naturally focus on the regions of highest strain rate and seismicity, such as the Himalaya, Alaska, and California. A consistent finding is that the tectonics are structured and guided by established faults of very low strength (e.g., *Kong and Bird* [1996], *Bird* [1996], and *Bird and Kong* [1994], respectively, on these three regions). Assuming hydrostatic pore pressure, the effective friction in these master faults is below 0.2, while that of the less deformed blocks between them is approximately 0.85 [e.g., *Byerlee*, 1978; *Kirby*, 1983, 1985]. There are several ideas concerning possible mechanisms of fault weakness (low-friction minerals in fault gouge; permanent high pore pressure in fault gouge; transient high pore pressure due to frictional heating; seismic slip under dynamically reduced normal stress at a boundary between materials of different shear modulus, etc.). However, there is no consensus about the relevant physics, and this is a barrier to progress in quantitative tectonics.

[3] One promising approach may be to study regions in which new plate boundaries are forming, where strains are still low, and faults might be expected to be undergoing a transition to low strength. Such places may sometimes be found where a plate boundary passes through, or near to, the Euler pole for that pair of plates (unless the Euler pole itself has moved from another site). *Gordon* [1995] and *Bird* [2003] identified several such places: the Laptev Sea region on the Eurasia-North America plate boundary; the Palau region on the Philippine Sea-Caroline plate boundary; the west central Atlantic region on the North America-South America plate boundary, the Chagos region on the India-Australia plate boundary, and southern Africa on the Africa-Somalia plate boundary. (Note that the plate we call ''Africa'' is called ''Nubia'' by some other authors.) Of these, the only subaerial region is southern Africa.

[4] Southward propagation of rifting is seen throughout the east African region. The modern East Africa rift (Figure 1) probably initiated between about 32 and 25 Ma, as indicated by flood basalt volcanism [*Berhe et al.*, 1987; *Baker et al.*, 1996; *Hofmann et al.*, 1997] on the central

[1]Department of Earth and Space Sciences, University of California, Los Angeles, California, USA.
[2]Department of Geological Sciences, University of Cape Town, Rondebosch, South Africa.
[3]Also at Department of Geophysics and Planetary Sciences, Tel Aviv University, Tel Aviv, Israel.
[4]Also at Institute of Geophysics and Planetary Physics, University of California, Los Angeles, California, USA.
[5]South African Nuclear Energy Corporation, Pretoria, South Africa.
[6]Also at School of Geosciences, University of the Witwatersrand, Wits, South Africa.
[7]Geological Survey of Norway, Trondheim, Norway.

Copyright 2006 by the American Geophysical Union.
0148-0227/06/2005JB003882$09.00

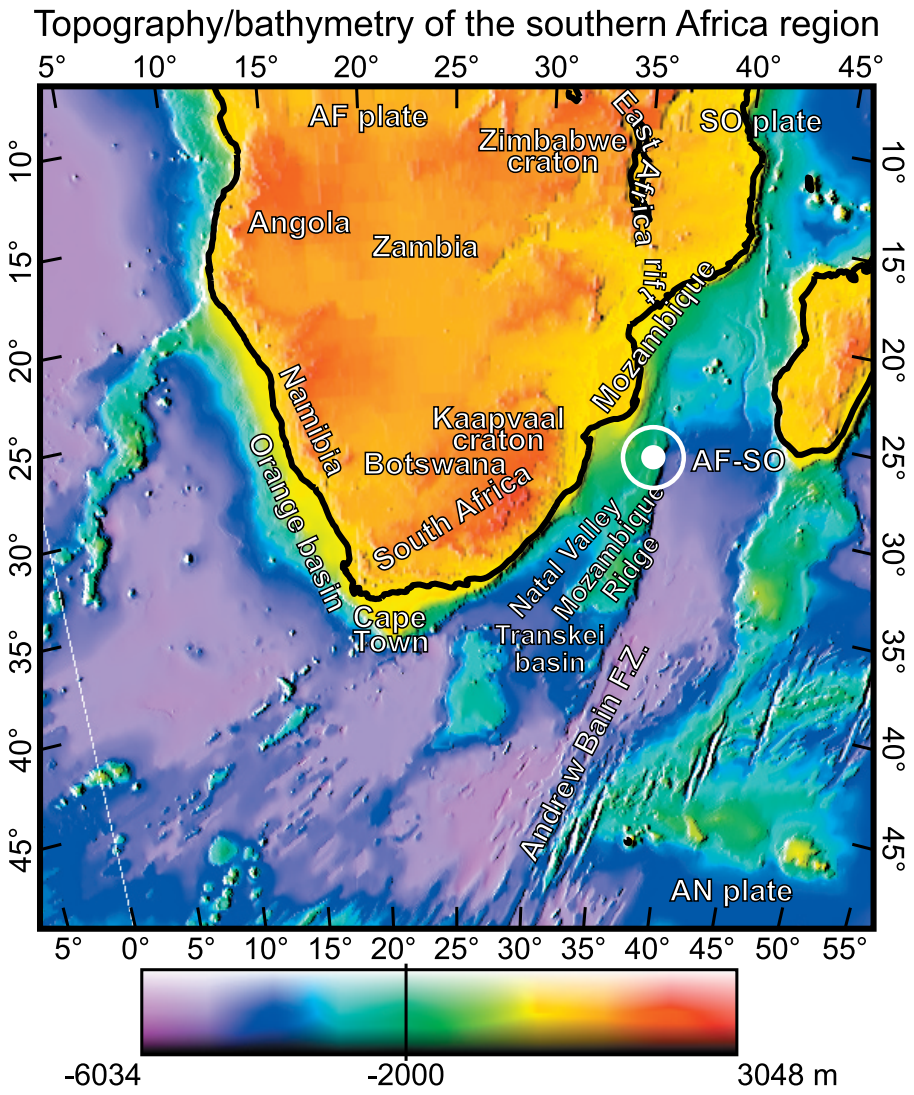

Figure 1. Topography and bathymetry of the southern Africa region, identifying places mentioned in the text. Plate abbreviations are AF Africa, SO Somalia, AN Antarctica. Circled dot AF-SO is the estimated Euler pole of *Chu and Gordon* [1999]; for other estimates, see *Fernandes et al.* [2004] and *Horner-Johnson et al.* [2005]. ETOPO5 topography of *NOAA* [1988].

Ethiopian plateau and the future sites of the Red Sea, Gulf of Aden, the northern Main Ethiopian rift, and the East Africa rift [*Ebinger et al.*, 2000]. Extension in southern Ethiopia and northern Kenya is younger than 25 Ma [*Morley et al.*, 1992; *Bosworth and Morley*, 1994]. *Ebinger et al.* [2000] argue that the Main Ethiopian rift and Eastern rift have propagated southward.

[5] Southern Africa is also good for such studies because it has had a relatively long period of tectonic quiet preceding this reactivation. The geologic history of the region includes the late Archean assembly of the Kaapvaal craton with Zimbabwe craton (Figure 1) along the Limpopo belt, intrusion of the Bushveld igneous complex at ~2 Ga, the addition of Proterozoic fold and thrust belts on the south (Namaqua-Natal) and west (Gariep-Kaoko), formation of the Cape Fold Belt on the south in a late Paleozoic orogeny, and Jurassic flood basalt eruption, rifting, and seafloor spreading on the western continental margin. On the southeastern margin, a Cretaceous event involved a complex mixture of transform tectonics and normal sense reactivation of late Paleozoic thrust faults [*de Wit and Ransome*, 1992].

[6] Within the area of the present study, poorly understood Late Cretaceous tectonic activity is expressed by the >240 km Waterberg thrust in central Namibia, tentatively dated at ~70 Ma [*Raab et al.*, 2002; *Viola et al.*, 2005]. This structure caused crustal shortening in a NNW-SSE direction, producing a stratigraphically inverted tectonic stack comprising an upper nappe of Late Proterozoic Damara gneisses (thickness > 150 m), a middle nappe of Triassic sediments (~16 m thick) and a lower unit of Jurassic sandstone and basalt [*Marsh et al.*, 2004].

[7] However, the only Tertiary tectonic process other than rift extension has been an accelerating regional uplift, possibly due to inferred upwelling mantle flow that originates at the core-mantle boundary and slants upward to the East Africa rift region [*Ritsema et al.*, 1999; *Gurnis*, 2001; *Ni et al.*, 2002; *Ni and Helmberger*, 2003a, 2003b; *Behn et*

Table 1. Most Compressive Horizontal Principal Stress Azimuths and Stress Regimes in Southern Africa[a]

Key	Latitude, deg	Longitude, deg	σ_{1H} Azimuth	Type	Quality	Regime	Depth, km	Site	Source
1	−34.783	19.633	115	GFS	A	NF	0	Gansbaai-Quoin Point, South Africa	*Andreoli et al.* [1996]
2	−35.170	22.150	145	BO	B	NF	0	Bredasdorp Basin, offshore South Africa	*Andreoli et al.* [1996]
3	−30.200	18.400	148	GFS	A	NF	0	Santab se Vloer normal faults, Bushmanland	*Brandt et al.* [2005]
4	−24.700	16.000	172	GFS	A	NS	0	Hebron dextral-normal fault, Namibia	*Viola et al.* [2005]
5	−19.900	21.900	40	GFS	A	NF	0	Gumare fault, Okawango Delta, Botswana	*McCarthy et al.* [2002]
6	−19.640	23.600	39	GFS	A	NF	0	Kunyere Fault, Okawango Delta, Botswana	*McCarthy et al.* [2002]
7	−19.680	23.800	42	GFS	A	NF	0	Thamalakane Fault, Okawango Delta, Botswana	*McCarthy et al.* [2002]
8	−17.417	14.250	173	OC	A	TF	0.134	Ruacana Power Sta. RSM 7 and 8, Namibia	*Stacey and Wesseloo* [1998]
9	−24.000	34.500	0	GFS	B	NF	0	Funhalouro-Mazenga Graben, Mozambique	*Ferro and Bouman* [1987]
10	−30.350	15.100	145	GFS	A	SS	0	offshore sinistral(?) "mud volcano" fault	*Viola et al.* [2005]
11	−26.500	17.600	167	GFS	A	NS	0	Dreylingen-Pfalz oblique-slip fault, Namibia	*Viola et al.* [2005]
12	−29.667	22.750	160	OC	A	SS	0.8	Prieska mine, Namaqualand	*Andreoli et al.* [1996]
13	−27.800	17.260	167	GFS	B	NF	0	Skorpion mine, Namibia	*Viola et al.* [2005]
14	−25.667	27.250	135	OC	C	NF		Rustenburg and Northam mines, Witwatersrand	*Andreoli et al.* [1996]
15	−29.700	17.900	145	OC	A	SS	1.57	Carolusberg mine, Springbok, Namaqualand	*Viola et al.* [2005]
16	−29.300	18.800	92	OC	A	SS	0.416	Black Mountain mine, Aggeneys, Namaqualand	*Viola et al.* [2005]
17	−21.383	15.367	152	GFS	B	TF	0	Otombawe-Elim-Vrede reverse faults, Namibia	*Klein* [1980]

[a]Not already in World Stress Map. Following conventions of the World Stress Map: Azimuth is measured in degrees clockwise from north. Type includes OC overcoring, GFS geologic fault slip orientation, and BO borehole breakout orientation. Quality standards were defined by *Zoback and Zoback* [1989]. Regime abbreviations are explained in text.

al., 2004; *Ni et al.*, 2005]. We believe that uplift and rifting may be related, and will attempt to incorporate possible shallow effects of this regional flow process in our models. However, an alternative view is that the uplift is controlled by the NE-SW trending Miocene-Pliocene Griqualand-Transvaal and Ciskei-Swaziland uplift axes that stretch across almost the whole South Africa-Swaziland region [*Partridge and Maude*, 2000], and that the uplift may therefore be related to horizontal compressive stress.

[8] We must expect that some ancient faults from previous orogenies in southern Africa will be reactivated by the present stresses. Evidence of Plio-Pleistocene fault reactivation is seen in Namibia [*Viola et al.*, 2005], the Cape Fold Belt [*Hill*, 1988; *Andreoli et al.*, 1996; *Dingle*, 1977; *Hatting and Goedhart*, 1997; *Goedhart*, 2000], Namaqualand [*Brandt et al.*, 2003, 2005] the Limpopo belt [*Brandl*, 1995; *Partridge and Maude*, 2000] and northern Natal [*Jackson and Hobday*, 1980; *Andreoli et al.*, 1996]. Therefore a full understanding of the strain rate field may require generations of research. In contrast, conservation of momentum requires the true stress field to be smoother, and we hope it will be easier to reproduce with simple models.

[9] In this paper we will make a start on the problem by identifying the most significant feature of the stress field in the southern Africa region, and attempting to reproduce it with finite element neotectonic models to determine its origin. The better models also make predictions of offshore stress fields, and of strain rate patterns, which may stimulate further research, although presently the data needed to test them are not available.

2. Regional Stress Directions and Stress Regimes

[10] Present stress directions in southern Africa have been obtained from in situ (overcoring) observations in mines, from seismic focal mechanisms, and from field observations of Holocene(?) faulting. Each type of indicator is potentially subject to bias: in situ data may not be fully corrected for the effects of mining, and earthquake ruptures and other Quaternary faults may follow existing planes of weakness which do not have the expected angle to the present principal stresses. Because all stress direction data are noisy [*Bird and Li*, 1996], with residuals of at least 18° between nearest neighbors, we can only expect to match broad trends in the data. It also follows that large numbers of redundant data are required for reasonable certainty that trends exist.

[11] "Stress regime" refers to the orientation of deformation produced, using an Andersonian classification into normal faulting (NF), strike-slip faulting (SS), and thrust faulting (TF). In some places, strike-slip faulting coexists with dip-slip faulting (because two principal stresses are equal, or the crust is anisotropic), so two additional regimes "NS" (predominately normal with strike-slip component) and "TS" (predominately thrust with strike-slip component) are also seen in the World Stress Map (WSM) database [*Reinecker et al.*, 2004].

[12] On the basis of data compiled into the WSM, there is a suggestion of a broad region extending from southwestern Angola to South Africa in which the most compressive horizontal principal stress direction ($\hat{\sigma}_{1H}$) is oriented NW to NNW. This area has been called the Wegener stress anomaly (WSA) [*Andreoli et al.*, 1996; *Viola et al.*, 2005]. *Viola et al.* [2005] tentatively speculated that it could result from ridge-push generated by the South West Indian Ridge.

[13] In Table 1, we collect 17 additional Holocene direction/regime data that are not widely known outside the region. This approaches the number of data (22) previously available from WSM. The new indicators support the proposed WSA stress direction province, and show that it extends from at least 16°S to 35°S along the western coast. The most intense horizontal compression within the WSA is in northwestern Namibia, where Andersonian conditions for thrusting are at least locally attained. Farther south, in parts of southern Namibia and Namaqualand, thrusting regime is no longer seen, and there is a mixture of the other regimes. The extent and stress regimes of the present-day WSA may be no older than Holocene, because in the late Pleistocene thrusting regimes were active in Namaqualand (about 70–13 ka; around 30°S/18.5°E) and south of the Wits basin (around 26°E/28.3°S).

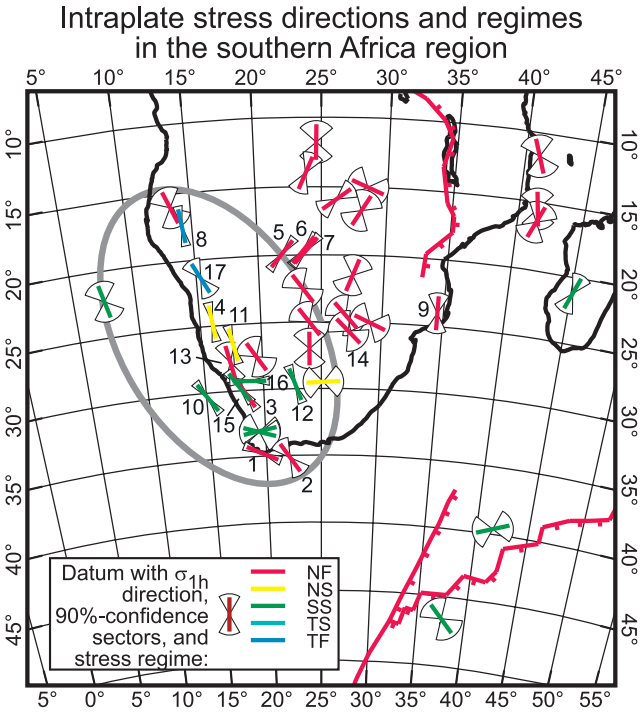

Figure 2. Intraplate indicators of stress regime (indicated by color) and azimuth of the most compressive horizontal principal stress ($\hat{\sigma}_{1H}$). Both data from the World Stress Map and data from Table 1 are shown; the latter have index numbers keyed to Table 1. We exclude all plate boundary data, using a more rigorous test than the WSM. The approximate region of the Wegener stress anomaly (Wegener stress direction province) is suggested by the ellipse.

[14] We have restricted our compilation of stress data (for scoring of finite element models) in two ways. First, we use only data from the southern part of the Africa plate (specifically, 10–50°S, 0–50°E), so that local processes are not overshadowed by effects of Africa-Eurasia collision [e.g., *Jimenez-Munt et al.*, 2001] in the north. Second, we use only intraplate data, according to a more restrictive definition than that used by the WSM. The WSM distinguishes some earthquakes as "plate boundary events," especially earthquakes on transform faults which represent established planes of weakness, rather than reliable indicators of intraplate stress. However, it does not so designate (and filter out) dip-slip earthquakes on spreading and convergent plate boundaries, as the authors of earlier editions of the WSM used to do. There are two problems with this newer editorial practice: (1) The value of focal mechanisms as stress direction indicators is greatest when new faults form in a homogeneous continuum, and least when slip occurs on established, inherited faults of low strength; unfortunately, the latter case is typical of plate boundaries. (2) The mid-ocean spreading ridges bounding our model are sites of young, thin, and weak lithosphere; an earthquake there may reflect only weak stresses of local origin which are difficult to model and not necessarily representative of plate-scale stress fields. In order to emphasize intraplate processes (and prevent them being swamped in statistics by more seismic plate boundary processes) we have applied a more rigorous filter: all data from within the wide plate boundary seismic zones as defined by *Bird and Kagan* [2004] have been excluded.

[15] All available intraplate data are shown in Figure 2. Within the WSA, all possible stress regimes are found inside the coastal belt, but inland to the east normal faulting is predominant. Some of the variety in stress regimes along the coast may be due to local effects of Mesozoic-Cenozoic flexure in response to erosion, as modeled by *Gilchrist et al.* [1994].

[16] A potential complication in the interpretation of stress regime data is the possibility of regime change with depth. The compilation of South African mine data (within 300 km of Johannesburg, within the Kaapvaal craton) by *Stacey and Wesseloo* [1998] shows a tendency for the vertical stress to equal the mean horizontal stress (SS regime) or exceed the maximum horizontal stress (NF regime) at more than 1 km depth, but for horizontal compression exceeding vertical (TF regime) to be observed closer to the surface. It is possible that weathering and stress relief microcracking may expand the volume of surficial rocks enough to generate an isotropic horizontal compression and cause a change to TF regime at shallow depth in some localities. We may hope, however, that the effect would be sufficiently isotropic to leave the azimuth of $\hat{\sigma}_{1H}$ relatively unaffected.

3. Finite Element Model Construction

[17] Modeling experiments were conducted with program Shells, which was introduced by *Kong and Bird* [1995]. Shells has been used for both global [*Bird*, 1998; *Bird and Liu*, 1999] and regional studies [e.g., *Jimenez-Munt et al.*, 2001; *Negredo et al.*, 2002; *Liu and Bird*, 2002a, 2002b]. It uses a thin shell approximation to model neotectonics of the lithosphere, based on estimated structure and temperatures, estimated rheology, and the conservation of momentum. Elastic strain is neglected, and therefore the velocities and strain rates predicted should be considered as quasi-static long-term averages.

[18] Shells does not take account of any strains or stresses caused by differential vertical movements or flexure of the lithosphere. Except around the outer rises of subduction zones, such flexural strains are generally thought to play a second-order part in orogenies. However, in more stable continental regions of smaller strain rate, it is less clear that flexure due to erosion, deposition, and/or postglacial rebound can be neglected. For example, *Gilchrist et al.* [1994] have modeled several kilometers of Mesozoic-Cenozoic uplift of the coastal belt of southwestern Africa in response to headward erosion of the coastal escarpment. This process is unfortunately not included in any of our models.

[19] Lithosphere structure in the Shells model consists of two compositional layers (crust and mantle lithosphere) which vary laterally in thickness. The lithosphere-asthenosphere boundary is assumed to be an isothermal surface. The asthenosphere has the same composition as the mantle lithosphere, but its geotherm is approximated by a single adiabat (so that it contains no lateral density variations). Geotherms within the lithosphere are assumed to be in conductive steady state, allowing them to be computed

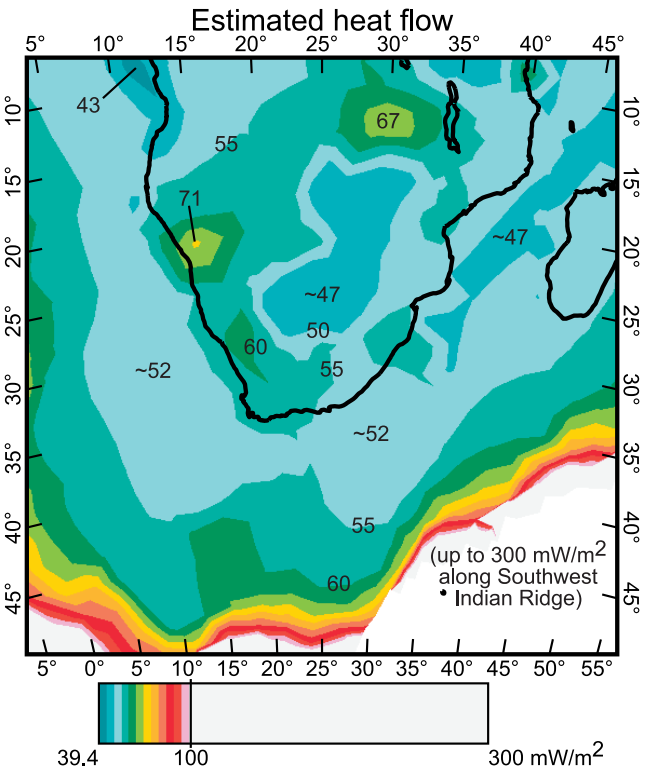

Figure 3. Map of estimated heat flow. Contour interval is 5 mW m^{-2}. Values up to 300 mW m^{-2} along the Southwest Indian Ridge spreading center are allowed to go off-scale, so as to display small variations within southern Africa and its continental margins.

from surface heat flow, crust and mantle conductivity, and crust and mantle radioactivity.

[20] The map of estimated heat flow used in this project (Figure 3) is a composite. Gridded seafloor ages from *Mueller et al.* [1997] were combined with the boundary layer model of *Stein and Stein* [1992] to estimate oceanic heat flow. On land, heat flow observations tabulated by *Pollack et al.* [1993] were inverted, interpolated by kriging, and then reinverted. (The inverse of heat flow is roughly proportional to lithosphere thickness, and its distribution is closer to Gaussian than the distribution of heat flow.) This model has the East Africa rift running along a belt of elevated heat flow (50–60 mW m^{-2}) at most latitudes, although it does not pass through two regions of higher heat flow (up to 75 mW m^{-2}) which are east of the rift in the Nairobi region (~0°N, 36°–42°E) and west of the rift in the eastern Zambia region (~13°S, ~30°E). (Both of these warmer spots are based on field data, and are not artifacts of interpolation.) The elevated heat flow in Namaqualand is based only on published data compiled by *Pollack et al.* [1993]; however, additional unpublished data in preparation (heat flows 59–81 mW m^{-2}; surface heat production 27–420 $\times$ 10^{-7} W m^{-3}) support this feature.

[21] Both fault and continuum elements have a frictional upper layer. Friction follows the Mohr-Coulomb law, and in continuum elements we assume that faulting is always on distributed sets of conjugate microfaults. Pore pressure assumed to be hydrostatic everywhere. The friction in continuum elements is always 0.85 [*Byerlee*, 1978], but in fault elements it is typically set lower. The high-temperature dislocation creep rheologies of both crust and mantle are thermally activated and nonlinear (n = 3). The mantle creep strength is based on olivine, as summarized by *Kirby* [1983]. The crustal creep strength is loosely based on quartz but was calibrated by *Bird and Kong* [1994] to be consistent with maximum earthquake depths in California.

[22] Because the continent-ocean transition will be seen to have important effects on computed stress fields, it is important to state that the Shells modeling approach makes no a priori or clear-cut distinction between continental and oceanic lithosphere. Only one type of crust is modeled (by a set of densities, creep strengths, and other properties distinct from those of the mantle). However, it is true that where this crust is thick (in continents and their margins) the lithosphere is computed to be weaker than oceanic lithosphere with equal heat flow. This follows from the relative weakness of quartz-like crustal dislocation creep rheologies at 300–800°C compared to the olivine dislocation creep rheology used to represent the mantle.

[23] Crust and mantle lithosphere thicknesses were computed from ETOPO5 topography (Figure 1) [*NOAA*, 1988] by assuming local isostasy of every vertical column with respect to mid-ocean spreading ridges, with 2.7 km of water and 5 km of crust overlying normal asthenosphere. (While small departures from isostasy, measured by the isostatic gravity anomaly, may exist locally, the two-dimensional (2-D) F-E code in Shells is not able to model stress fields dominated by flexural rigidity effects.) An iterative method was used in the calculation, because adjustments in Moho depth affect not only the isostatic balance, but the geotherm as well. In the end, the continent-ocean transition in strength alluded to previously is almost entirely controlled by the map of bathymetry, which is of course the best known field.

[24] Thermal, density, and rheologic parameters were as described by *Liu and Bird* [2002b], except that crustal radioactive heat production was reduced from 6.2 $\times$ 10^{-7} W m^{-3} to 4 $\times$ 10^{-7} W m^{-3} (contributing 14 mW m^{-2} of heat flow where crustal thickness is 35 km) in order to more closely approximate the crustal thicknesses in the CRUST2 model [*Bassin et al.*, 2000]. The result was that our computed lithosphere thickness varied up to a maximum of 120 km in the Kaapvaal and Zimbabwe cratons in southern Africa. (Since our model of variations within the mantle is purely thermal, and does not include compositional variations, it is difficult to compare this with the thicknesses of 160–370 km determined by *James et al.* [2001] and *Niu et al.* [2004] for the Fe-depleted chemical boundary layer under the Kaapvaal craton.)

[25] Lateral boundary conditions for a regional model can be fixed velocity or fixed traction. The type of fixed traction used in this study was always lithostatic normal traction with no shear traction.

[26] Some previous authors have speculated that stress directions in southern Africa may be related to "absolute velocity" of the region. Our calculations were carried out in the AF (Africa plate) reference frame, but since Shells was designed to be invariant with respect to Eulerian rotations [*Kong and Bird*, 1995], this choice has no effect on the strain rates or stresses in any simulation. We infer that these speculations were actually directed toward possible effects of *relative* velocity with respect to the transition zone or

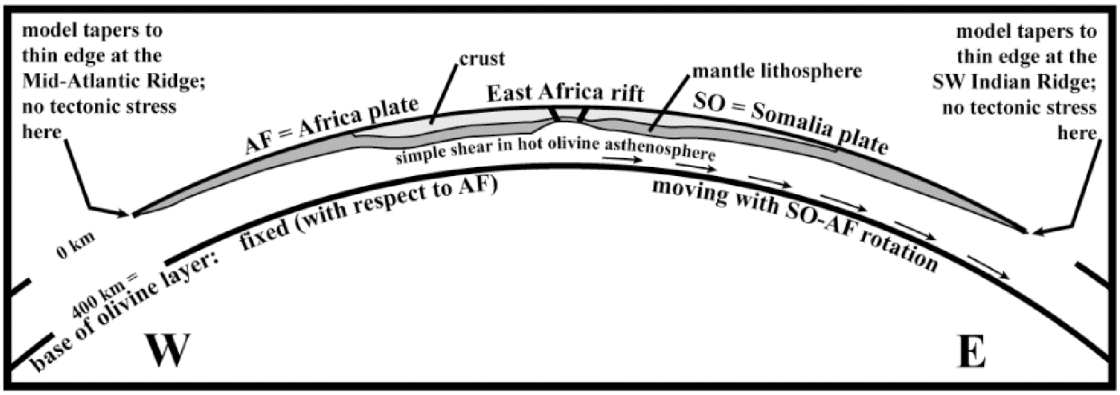

Figure 4. Schematic cross section of the model along an east-west great circle, showing how the velocity field on the surface is linked to an assumed velocity field at a depth of 400 km, through the rheology of a hot olivine asthenosphere. In the early models this deep velocity field was assumed to be uniformly static with respect to northwest AF. In later models a divergent flow (shown here) was assumed to drive (or permit) relative rotation of SO with respect to AF. Thicknesses of crust and mantle lithosphere are generic and not to scale.

lower mantle, which can introduce important shear tractions on the base of the lithosphere. Accordingly, we have tested two alternate cases: transition zone uniformly static with respect to AF; or, transition zone diverging under the East Africa rift, as in the two-plate (AF, SO) surface velocity model of *Bird* [2003].

[27] Basal traction is always lithostatic in the vertical direction. In the horizontal plane, shear traction components are computed from the rheology of a hot olivine asthenosphere and the relative motion (simple shear) between the model lithosphere and an assumed map of mantle flow at 400 km depth, in the transition zone (Figure 4). We always assumed an asthenosphere temperature of 1200°C at 100 km depth, which has been shown to give reasonable amounts of subcontinental traction in global models (e.g., model 97001 of *Bird* [1998]). At this temperature, subcontinental tractions are typically 0.2 MPa at relative velocity 0.1 mm yr^{-1}, increasing to 0.8 MPa at relative velocity 6 mm yr^{-1}. (The relation is nonlinear because the dislocation creep flow law of olivine is nonlinear, with $n = 3$.)

[28] Once each model calculation is iterated to convergence, it predicts long-term average surface velocities, anelastic strain rates, fault slip rates, and stresses. Because the continuum elements were assumed to be isotropic, the predicted principal stress axes have the same directions as the principal axes of surface strain rates. The predicted stress regime (actually strain rate regime) is determined by the orientations of the principal strain rate axes: normal faulting occurs where the most compressive principal strain rate axis $\dot{\hat{\varepsilon}}_1$ is vertical, strike-slip faulting occurs where $\dot{\hat{\varepsilon}}_2$ is vertical, and thrust faulting occurs where $\dot{\hat{\varepsilon}}_3$ is vertical. Following this rule, we have no objective basis for distinguishing the mixed regimes NS and TS that are sometimes reported in the WSM data set. To accommodate this discrepancy, we treat any NS datum as consistent with any model prediction of negative vertical strain rate and two horizontal principal strain rates of opposite sign. We treat any TS datum as consistent with any model prediction of positive vertical strain rate and two horizontal principal strain rates of opposite sign.

[29] The convention of Shells, and this paper, is that compressive normal stress components are numerically negative, and tensile stress components are numerically positive. In order to best display the stress fields predicted by the Shells models, we emphasize their useful information in two ways. First, we define the "tectonic stress tensor" as the difference between the stress tensor at any point and a reference pressure at the same depth (relative to a geoid) beneath a mid-ocean spreading ridge with no strength. As in the isotatic calculation above, the reference pressure is computed in a structure of layered fluids: 2.7 km of seawater over 5 km of crust over asthenosphere. This takes out the depth-dependent (but not laterally varying) pressure component that would otherwise overwhelm the plots. Second, we vertically integrate the tectonic stress tensor through the lithosphere. This is a natural step because, under the assumptions and simplifications of the Shells modeling method, the tectonic stress tensor does not rotate with depth (within the lithosphere). The resulting map patterns of vertical integrals of tectonic stress tensors are constrained to satisfy the vertical integral of the momentum equation (with density anomaly substituted for total density), and are expected to be smooth (assuming that basal shear tractions on the lithosphere are not huge).

[30] In plots, we represent the horizontal principal components of the vertical integral of the tectonic stress with pairs of diverging arrows (where the corresponding principal value is positive) or converging arrows (where the principal value is negative). For the vertical component, triangles are used to represent positive principal values, and circles are used to represent negative principal values. Generally, ocean floor deeper than 2.7 km will display triangles, whereas shallow ocean and land areas will display circles. The size of the triangle or circle depends on the topography (difference from reference ridge depth of 2.7 km) and on the depth and mode of compensation of this topography anomaly. (This one component can be computed from the density structure alone, without considering strain rates or deviatoric stresses.) However, the sign of the vertical component is not the only factor in determining stress regime

Table 2. Misfits of Shells F-E Models of Neotectonics in the AF and SO Plates, Scored by Their Stress Predictions in the Southern Africa Region

Model	Density and Thermal Structure?	Plate Edges	Basal Drag	East African Rift?	Friction in Fault Elements	Mean Azimuth Error		Incorrect Regime	
						WSM (n = 22)	New Data (n = 17)	WSM (n = 22)	New Data (n = 17)
AF-SO-001	3-D	lithostatic pressure	resistive	no; strong	(no fault elements)	40°	34°	59%	59%
AF-SO-002	3-D	lithostatic pressure	resistive	yes; to 21°S	0.1	40°	34°	59%	59%
AF-SO-004	3-D	lithostatic pressure	resistive	yes; to 21°S	0.0	40°	32°	73%	59%
AF-SO-013	3-D	lithostatic pressure[a]	active (PB2002)	yes; to 21°S	0.1	33°	30°	32%	41%
AF-SO-014	3-D	lithostatic pressure[a]	active (PB2002)	yes; to 21°S	0.0	41°	27°	68%	59%
AF-SO-015	1-D	lithostatic pressure[a]	active (PB2002)	yes; to 21°S	0.1	25°	35°	18%	35%
AF-SO-016	3-D	lithostatic pressure[a]	active (HJ2005)	yes; to 21°S	0.1	36°	32°	41%	41%
AF-SO-017	1-D	lithostatic pressure[a]	active (HJ2005)	yes; to 21°S	0.1	26°	20°	9%	47%

[a]Spreading of East Africa rift enforced by setting ESE velocity of one node in northern SO plate to 6 mm yr^{-1}. HJ2005, *Horner-Johnson et al.* [2005].

(Andersonian faulting regime): to predict this, it is necessary to compare the vertical principal value with each of the two horizontal principal values. The circle symbol (used for negative vertical principal values, on land) is intended to make this comparison as easy as possible. For example, when a figure shows a circle for the vertical component, and converging arrows for both horizontal components, but the circle is larger in radius than both pairs of horizontal component arrows, the stress regime would be NF, and the predicted horizontal extension direction would be that with the smallest (weakest) pair of converging arrows.

4. Model Experiments

[31] The eight models discussed here are summarized in Table 2. All included the same spatial domain: the complete extent of the Africa and Somalia plates [*Bird*, 2003]. All had the same ''free'' lateral boundary conditions; that is, shear traction was zero and normal traction was lithostatic. This is a reasonable approximation of the hot, weak spreading rises that surround the southern Africa region. Also, this approximation allows us to avoid selecting particular Euler poles for the relative motions of the Eurasia, Arabia, India, and Australia plates, all of which have been controversial.

4.1. Lateral Variations in Density Moment

[32] The first model (AF-SO-001) had no explicit representation of the East Africa rift, and its lower mantle was assumed to be static with respect to northwest Africa, so the basal boundary condition resisted all horizontal velocities with respect to the AF frame. In fact, there was no source of deviatoric stress in this model other than the lateral variations of density within the lithosphere. In a thin shell model like this, the important scalar measure of density structure is the ''density moment'' [*Fleitout and Froidevaux*, 1982; *Turcotte and Schubert*, 2002, p. 217] which is the vertical integral, through the lithosphere, of density multiplied by elevation (or by depth). (Note that these two alternate definitions result in differences of opposite sign for any given pair of density structures.) This measure varies laterally even for isostatic models, and this gives rise to such effects as ''ridge-push'' (horizontal compression in old seafloor adjacent to a spreading rise) and ''continental collision resistance'' (horizontal compression in normal continent adjacent to an elevated mountain range).

[33] We found that the regional high elevations and high heat flows along the East Africa rift generated some spontaneous spreading in this model, with relative rotation about a pole near Cape Town. However, it was very slow (0.0016° Myr^{-1}), with relative SO-AF velocities of no more than 0.1 mm yr^{-1} at the north end of the rift in Ethiopia, where the actual spreading rate is believed to be closer to 6 mm yr^{-1} [*Chu and Gordon*, 1999] based on marine magnetic anomaly data, or 7 mm yr^{-1} [*Fernandes et al.*, 2004] based on geodetic data.

[34] In the southern Africa region, the highest density moments are in the elevated continental plateaus, so these were predicted to spread laterally. Consequently, the continental regions were almost all predicted to be in the NF regime (Figure 5). The strong belt of old oceanic lithosphere just offshore restricted this spreading tendency, and it experienced much higher stress intensities, with primarily SS regime close to the continental margin, and TF regime farther offshore. The general direction of $\hat{\sigma}_{1H}$ in offshore regions was radial (pointing toward Botswana), and the general direction of $\hat{\sigma}_{2H}$ was circumferential. Table 2 shows that the fit of predicted stresses was poor: 59% of the regimes were incorrect, and the mean azimuth error in $\hat{\sigma}_{1H}$ was 34–40°. (Since the largest possible azimuth error at any point is 90° by definition, a mean azimuth error of 45° would be expected when comparing completely random predictions to data.)

4.2. Adding a Weak East Africa Rift

[35] In the second model (AF-SO-002), we introduced fault elements to represent the (arguably) well-established parts of the AF-SO plate boundary, which are the East Africa rift north of 21°S [cf. *Bird*, 2003, Figure 18], and the Andrew Bain fracture zone [*Lemaux et al.*, 2002] south of 37°S. These locations are shown in Figures 1 and 2. The East Africa rift was modeled with normal faults of 65° dip. Because the Andrew Bain fault zone initiated as a strike-slip transform fault but may now be reactivated as a thrust, it is not clear what dip is appropriate; we assumed 45°. The friction assigned to these fault elements was 0.10, which is substantially less than the continuum friction of 0.85 [*Byerlee*, 1978], but comparable to levels inferred for established plate boundary faults in previous models of other regions. For example, *Kong and Bird* [1996] inferred effective fault friction of 0.085 in the Himalaya-Tibet orogen; *Bird* [1996] inferred effective fault friction of ~0.17 in Alaska; and *Bird and Kong* [1994] inferred effective fault friction of 0.12–0.25 in California, which was confirmed by *Geist and Andrews* [2000].

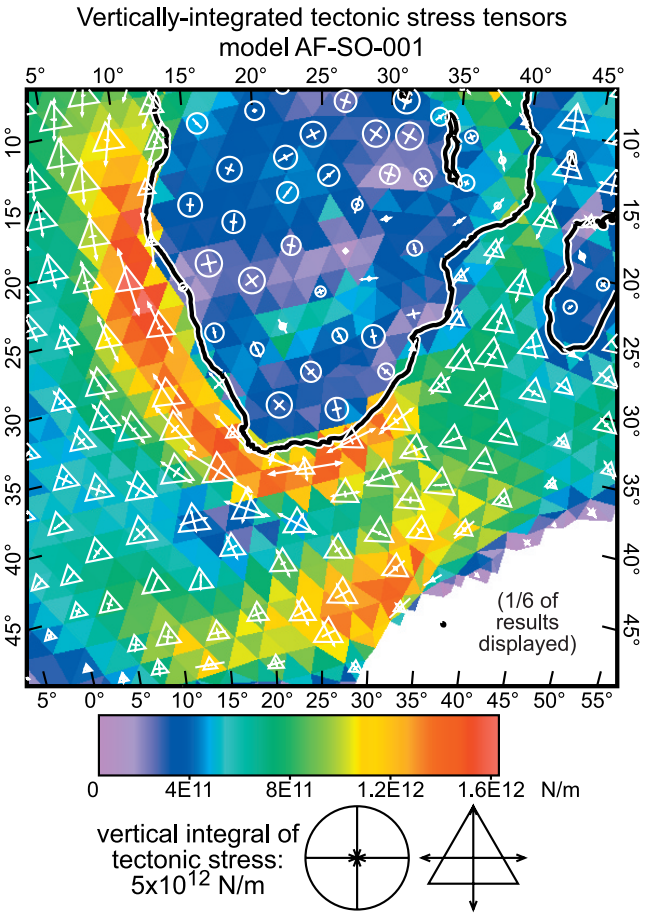

Figure 5. Vertical integrals, through the model lithosphere, of the tectonic stress tensor (symbols) and of the greatest shear stress (colors), for model AF-SO-001. This particular model stress field is almost entirely due to lateral variations in density moment. The "tectonic stress tensor" is defined as the total stress tensor minus the lithostatic pressure expected at the same elevation beneath a mid-ocean spreading ridge with no strength. Circles show negative vertical components of the vertical integrals of tectonic stress (on land and in shallow water), and triangles show positive vertical components of the vertical integral of tectonic stress (in ocean basins deeper than the reference spreading ridge). Tensor symbols for vertical integrals of tectonic stress are scaled by radius (not area), and the reference symbols in the margin portray isotropic compression and tension, respectively.

[36] Surprisingly, relative AF-SO plate rotation was virtually unchanged in this model (0.0016° Myr^{-1}; maximum spreading velocity 0.1 mm yr^{-1}). This was because the assigned fault friction was only low enough to cause significant fault slip rates in two segments of the rift: central Ethiopia (7°–10°N; up to 0.14 mm yr^{-1}), and the Lake Albert-Lake Tanganyika segment (2°N–7°S; up to 0.057 mm yr^{-1}). The model heave rates (horizontal components of slip rates) at these localities were $\leq$0.06 and $\leq$0.024 mm yr^{-1}, respectively. At other latitudes, extension occurred in the continuum elements adjacent to the defined rift, especially around the longitudes of highest heat flow. Since the velocity and strain rate fields in southern Africa were unchanged, the predictions of stress directions and regimes were unchanged from the previous model, and continued to be unacceptable (Table 2).

4.3. Elimination of Frictional Resistance in East Africa Rift

[37] In another model (AF-SO-004) we completely eliminated friction on the assigned East Africa rift faults and the Andrew Bain fracture, causing them to behave much like magma-filled cracks. (That is, they transmit normal tractions equal to local lithostatic pressure, but no shear tractions or anomalous normal tractions.) The reasons for such a model were (1) to accelerate the relative rotation of SO with respect to AF and (2) to simulate the stress concentration expected around the tips of frictionless cracks.

[38] SO-AF spreading was in fact accelerated, to 0.009° Myr^{-1} (with pole near 37°S, 22°E, giving maximum differential velocities of 0.6 mm yr^{-1} in Ethiopia). This is still an order of magnitude less than the actual rate, presumably because of the resistance coming from basal shear tractions in this model. Virtually all of the relative velocity appeared as heave rate on the frictionless faults, as expected, with heave rates tapering linearly to zero at their blunt ends in the southern Africa region. Stress concentrations were created around each crack tip, up to about 5$\times$ the level of deviatoric stress in distal regions. (The stress singularity expected at a crack tip in a plate of power law rheology has a small radial exponent, but even so, our finite element grid is not able to resolve its fine detail.) The principal effect on the directions of predicted stresses and their regimes was to superpose two local crack tip stress fields: at the south end of the East Africa rift there was a NF regime with radial tension, and at the north end of the Andrew Bain fracture there was a TF regime with radial compression. Table 2 shows that the fit to azimuths of new data improved from 34° to 32°, but incorrect regimes with respect to WSM data increased from 59% to 73%, so there was no overall improvement, and the model remained a poor match to available data.

4.4. Imposed SO-AF Spreading at Realistic Rates

[39] It appears that variations in the density moment of the lithosphere are insufficient to drive AF-SO relative motion in the East Africa rift against the resistance of passive upper mantle, and that driving forces must be supplied on the model boundaries. For the remaining models, we modified the boundary conditions in two ways to force realistic rates of relative rotation between SO and AF. First, the map of horizontal velocities assumed beneath the asthenosphere was changed to be equal to the surface velocity map of the *Bird* [2003] plate model. Surprisingly, this resulted in basal tractions ($\sim$0.3 MPa) below the northern part of SO that were still directed to the northwest; this means that the new basal boundary condition was still resisting spreading, rather than driving it. Second, to further regulate the spreading rate, an ESE-ward velocity of 6 mm yr^{-1} was imposed at a single boundary node in the northern part of the SO plate (at 4°N, 52°E, in a strong region of low heat flow). This is a very crude simulation of velocity regulation which may actually involve interactions

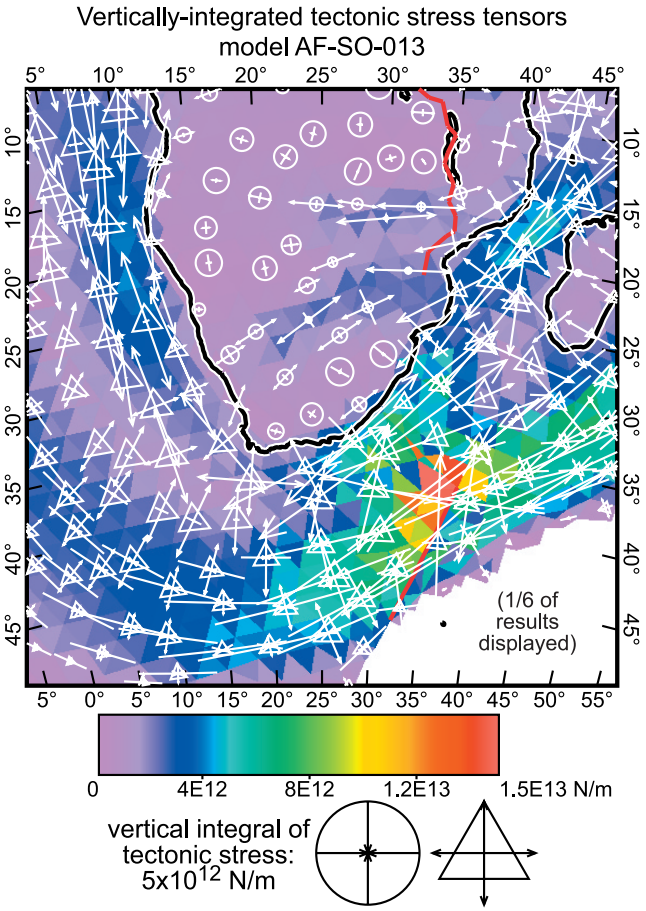

Figure 6. Vertical integrals, through the model lithosphere, of the tectonic stress tensor (symbols) and of the greatest shear stress (colors), for the preferred model AF-SO-013. Conventions are as in Figure 5. This model stress field also includes effects of lateral variations in density moment but is dominated by relative rotation of SO with respect to AF, which is set to realistic rates using basal tractions and one distant velocity boundary condition.

with all the neighboring plates (AR, IN, AU). However, since we do not score model predictions of stress in the northern SO region and do not display it in our figures, the artificial stress concentration around this single node probably will not affect model scores, nor mislead readers.

[40] In the first of this new set of models (AF-SO-013), we reverted to representing the East Africa rift and Andrew Bain fracture with fault elements of effective friction 0.1. The stress field of this model has its highest amplitudes offshore in strong oceanic lithosphere (Figure 6). Because of relative rotation of the SO portion with respect to the AF portion, there is a belt of very strong horizontal tension (up to 1×10^{13} N m^{-1}) close to the continental margin, and an outlying belt of horizontal compression. Both belts wrap around southern Africa into the southern Atlantic, running as far north as the equator, where they meet the African continental margin at right angles and merge. There is an additional local concentration of deviatoric stress at the north end of the Andrew Bain fracture (up to 1.5×10^{13} N m^{-1} of vertically integrated shear stress, or up to 3×10^{13} N m^{-1} for vertically integrated principal stress). However, there is no stress concentration at the southern tip of the defined East Africa rift fault elements, because in this model the southernmost faults were not active. On land in southern Africa, the primary stress field was one of NE-SW horizontal tension, which branches from the offshore oceanic belt of tension at the Indian Ocean margin in latitude range 15°–25°S, then passes southwest through the stronger regions of low heat flow, such as the Kaapvaal craton. (It continues offshore into the eastern Atlantic Ocean, but here this stress component is no longer σ_{2H}, but becomes σ_{1H} because there is an even stronger horizontal tension in the NW-SE direction.) The correlation of predicted and actual stress azimuths is now improved, at least on land and south of the equator (Figure 7). Table 2 shows that the overall misfit to southern African intraplate stress data has been significantly reduced (relative to AF-SO-002): incorrect stress regime predictions drop from 59% to 32–41%, while mean errors in $\hat{\sigma}_{1H}$ azimuth are reduced from 34–40° to 30–33°. An interesting suggestion of this model is that the Wegener stress direction province may be unified and organized more by SW-NE horizontal tension (σ_{2H}) than it is by NW-SE compression (σ_{1H}). (This point is better illustrated by Figure 6 than by Figure 7; this comparison shows the limitations of stress orientation data without magnitude information.)

[41] In model AF-SO-014, we kept the same boundary conditions, but reduced friction to zero on the East Africa

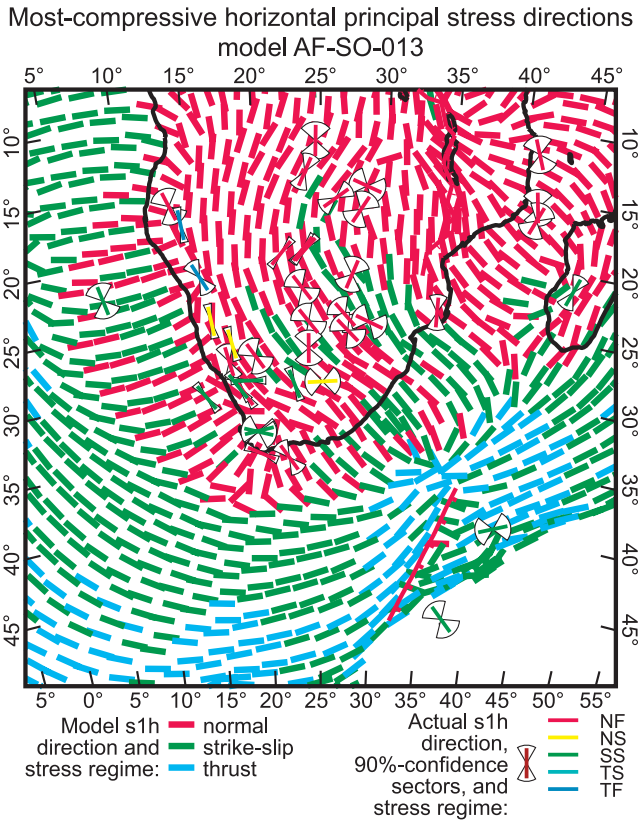

Figure 7. Most compressive horizontal principal stress directions from the preferred model, AF-SO-013, which is dominated by effects of relative plate rotation. Stress regimes (colors) are explained in text. Available data (with uncertainty fans) are from Figure 2.

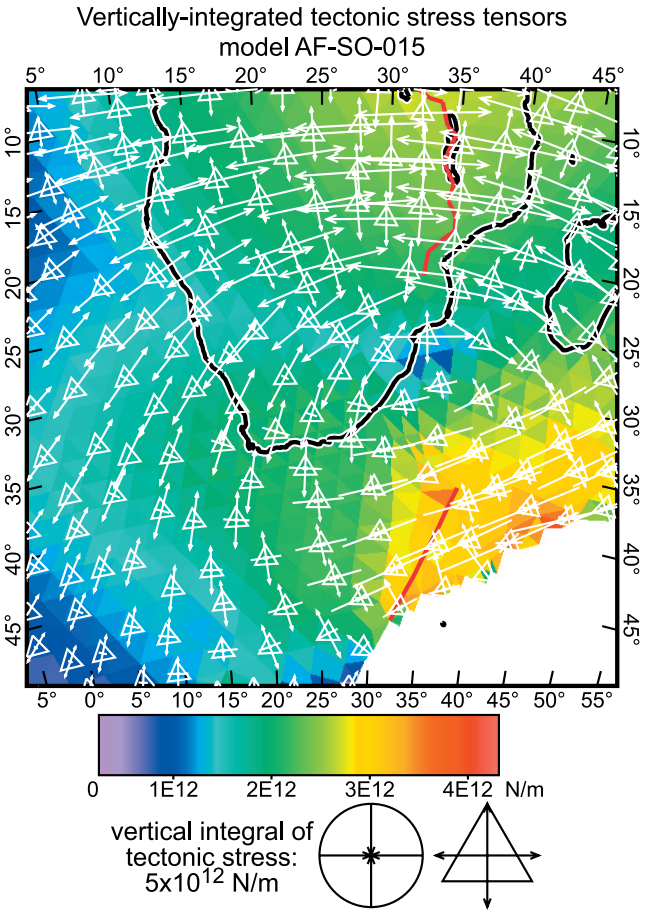

Figure 8. Vertical integrals, through the model lithosphere, of the tectonic stress tensor (symbols) and of the greatest shear stress (colors), for model AF-SO-015. Conventions are as in Figure 5. This model shows only the effects of relative rotation of SO with respect to AF because it includes no lateral variations in either lithosphere strength or density moment, except for the low-friction faults indicated along the East Africa rift and Andrew Bain fracture zone.

rift faults and Andrew Bain fracture. This internal free boundary had the effect of reducing deviatoric stresses to very low levels throughout continental Africa, except near the crack tip stress concentrations. Table 2 shows that the misfits of this model were comparable to those of AF-SO-004, which were unacceptable.

[42] The contrast between these two experiments shows the need for residual strength on the faults of the East Africa rift. While 0.1 is not necessarily the optimal friction level, we have seen that this friction allows a balance between localized slip on a few master faults and regionally distributed extension in adjacent crust. Such a balance is suggested by the widespread and diffuse seismicity of the East Africa rift, as well as by its complex map pattern of simultaneously active normal faults. Future high-resolution models of the rift should explore the hypothesis that effective friction may drop from ~0.85 to ~0.10 during the accumulation of the first few kilometers of net slip.

[43] One remaining concern is that our preferred model (AF-SO-013) predicts very high stress intensities offshore, where there are almost no data to test the model. Furthermore, it mispredicts the σ_{1H} azimuth at the "mud volcano" fault site [*Ben-Avraham et al.*, 2002; *Viola et al.*, 2005] (datum 10 in Figure 2) by 79°, as well as the regime. This led us to question whether the difference in strength between continental and oceanic lithosphere might be overestimated in these models. To test this, we computed a model (AF-SO-015) with a 1-D density and thermal structure. That is, it had no lateral variations in lithosphere strength, and also no lateral variations in density moment. The predicted stress field of this model (Figure 8) was extremely smooth, with horizontal tension almost circumferential about the Euler pole of SO-AF (on the north side) and horizontal compression almost circumferential about the same Euler pole (on the south side). Surprisingly, this simple model fits available data better (in three out of four columns in Table 2) than the preferred model AF-SO-013 (which we still consider to be more realistic). In particular, it fits inferred stress at the offshore mud volcano fault site.

4.5. Alternative Location of AF-SO Pole

[44] The AF-SO pole location shown in Figure 1 is that of *Chu and Gordon* [1999], which was also adopted by *Bird* [2003]. We used this to determine the pattern of mantle flow at 400 km depth in the models with "active" basal boundary conditions that were discussed above. Later, a very different AF-SO pole location (44.7°S, 2.8°E) was published by *Horner-Johnson et al.* [2005]. They based this on additional spreading rates and transform azimuths beyond those available to *Chu and Gordon* [1999]. On the other hand, they excluded data from the region near the *Chu and Gordon* pole (which had most strongly constrained its location) based on subjective arguments. An additional issue is that the newer pole is not consistent with data from the Red Sea and Gulf of Aden, requiring deformation of the Somalia "plate." Finally, the newer pole is not consistent with three thrust-fault focal mechanisms in the oceanic lithosphere near (36°S, 48°E; Figure 9) although the earlier Chu and Gordon pole was. Still, we tested in two additional models whether this revised pole location (translated into lower mantle flow patterns) would affect our results. Table 2 shows that model AF-SO-016 is the same as preferred model AF-SO-013 except for the change in pole position, while 1-D model AF-SO-017 is the same as 1-D model AF-SO-015 except for the change in pole position. Fortunately there was little change in overall scores in either experiment. Still, this points to the serious need for additional geodetic data to constrain the regional kinematics, before definitive results on dynamics can be expected.

5. Discussion

[45] The relative success of the simple 1-D strength models discussed above presents a dilemma: Is the improvement in stress predictions in southern Africa enough to offset laboratory results on the strength contrast between olivine and quartz, as well as many decades of qualitative observations that oceanic lithosphere appears to be more rigid than continental? This dilemma presents an opportunity for future research. If enough seismic, geologic, and even in situ stress data can be collected in the regions offshore from southern Africa, there is an opportunity to use

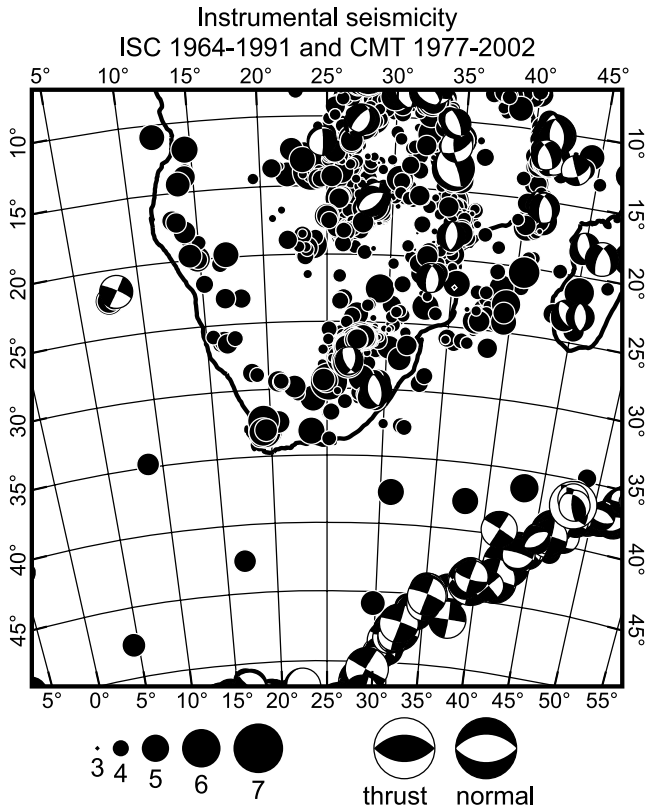

Figure 9. Instrumental seismicity of the southern Africa region, as recorded in two teleseismic catalogs: International Seismological Centre 1964–1991 (solid dots with no focal mechanism) and Harvard centroid moment tensor catalog 1977–2002 (''beach balls'' showing focal mechanisms on lower focal hemispheres). Note the much higher seismicity on land than at sea, which is better predicted by model AF-SO-013 (with lateral heterogeneities) than by model AF-SO-015 (without lateral heterogeneities).

neotectonic modeling to determine the correct contrast in strength between oceanic and continental lithosphere, and thus the relative dislocation creep strengths of crust and mantle.

[46] To summarize our experiments: The models presented here have deviatoric stress fields which are primarily due to three sources: (1) lateral variations in density moment; (2) resistance of unbroken lithosphere to relative rotation of SO with respect to AF; and (3) stress concentration near the tips of frictionless cracks.

[47] Unfortunately, it was not possible to display each source in isolation. Model AF-SO-001 which was intended to illustrate source 1 actually contained a bit of source 2 because variations in density moment drove very slow relative plate rotation even in the absence of a predefined crack. Source 2 cannot be illustrated in isolation because plate-like behavior will not occur without either variations in lithosphere structure (source 1) or a predefined weak rift (source 3). A model with only a frictionless crack could be created, but it would have no motion or stress without some contribution of sources 1 and/or 2.

[48] Nevertheless, we experimented with the relative importance of these 3 sources, and reached two conclusions. First, quality of the predicted stress field clearly improves with change of basal drag from passive to active, which increases the rate of relative rotation between SO and AF. Therefore we suggest that the Wegener stress direction province, and other features of the stress field in southern Africa, are primarily due to the resistance of unbroken lithosphere to relative plate rotation, with only minor contributions from the other sources (including ridge push). (However, since flexural effects were not incorporated in our models, there has been no testing of possible alternative flexural hypotheses.)

[49] Second, while the East Africa rift (north of 21°S) may have undergone significant strain weakening, it must have some residual strength (effective friction $\geq$0.1) to explain observed stress patterns and distributed deformation. Although it would be desirable to constrain the rift strength more precisely, it is doubtful that our present map of interpolated heat flow gives an adequate basis. We have found that there is a delicate balance between slip on a master normal fault of low friction and distributed extension in adjacent crust with higher heat flow. To accurately model this, we would need to significantly improve both the heat flow and fault maps.

[50] In the oceanic regions offshore from South Africa, our models indicate at least two different possible stress fields, and we are unable to choose between them because the available data are not sufficient. Recent studies have yielded evidence for neotectonic activity in the offshore areas. *Ben-Avraham et al.* [2002] reported the finding of mud volcanoes within the Orange Basin offshore of western South Africa (Figure 1 and Figure 2, datum 10). The mud volcanoes form a linear trend, striking N to NNW and crosscutting the regional isobaths at an angle of about 30°, which suggests that the trend is of tectonic origin. *Viola et al.* [2005] have placed the phenomenon of the mud volcanoes in this region in the broader structural/tectonic context of the Wegener stress anomaly, and demonstrated that the mud volcanoes are associated with active faulting.

[51] Marine studies of the Natal Valley and Transkei Basin (Figure 1) offshore of southeast Africa have indicated neotectonic activity across vast areas [*Ben-Avraham*, 1995; *Ben-Avraham et al.*, 1994, 1995]. Along the southeastern margin of the Natal Valley oceanic basin, near the northwestern margin of the Mozambique Ridge (Figure 1), the structural style of a deformation zone seen on seismic profiles indicates a positive or compressional flower structure along a strike-slip fault. Additional neotectonic deformation is also seen as unusual sill-shaped structures located near the center of the basin. The anomalous box-shaped structure has an apparent trend subparallel to the strike-slip faults identified in southeastern part of the basin. On the basis of this association, *Reznikov et al.* [2005] hypothesized that the sill-like structure is related to transpressional faulting and maybe out-of-plane folding. The origin of the sill-like structure is highly uncertain. Other interpretations such a laccolithic intrusion or an olistostrome are also plausible, and supported by gravity and magnetic data.

[52] The marine data in this area are relatively few and cannot provide information on the stress direction, but they clearly indicate tectonic activity. The model of *Chu and Gordon* [1999] which places the Euler pole of AF–SO relative motion near the southeastern African continental

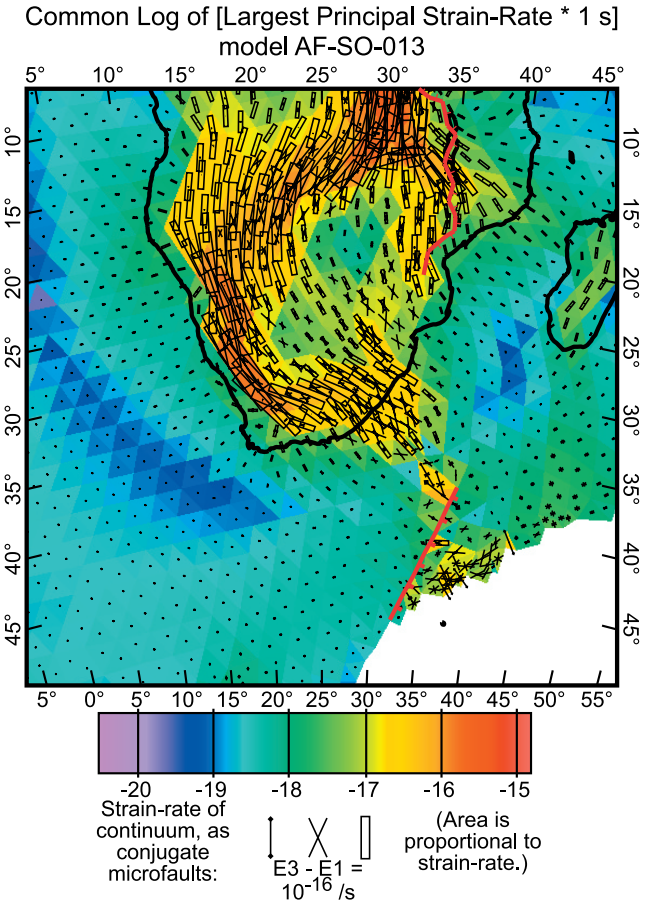

Figure 10. Long-term average (anelastic) strain rates predicted by the preferred model, AF-SO-013. Color indicates the common logarithm of the magnitude of the principal strain rate with greatest absolute value (in units of s^{-1}). Symbols show orientation of the strain rate tensor in terms of the strikes of conjugate microfaults predicted. Rectangles represent grabens (horizontal extension); dumbbells with diamond-shaped terminations represent thrust faults (horizontal shortening), and crosses indicate conjugate strike-slip faults (one sinistral and one dextral in each pair). There is a close relationship between this figure and the map of estimated heat flow (Figure 3).

margin in the Natal Valley predicts slow convergence in the oceanic area. This agrees with the evidence of transpression along the southeastern margin of the Natal Valley. On the other hand, evidence for possible extensional neotectonics and igneous intrusion in the area between the Agulhas Plateau and the Mozambique Ridge [*Ben-Avraham*, 1995; *Ben-Avraham et al.*, 1995] suggests a recent change in the stress regime in this area. The earthquakes of 1975 and 1981 within the Natal Valley [*Hartnady*, 2002] add strong support to the seismic reflection findings of neotectonic activity.

[53] One major reason for studying neotectonics in South Africa is to assess the seismic hazard, especially to mines and to sites of nuclear power generation and waste disposal. While our very preliminary model is certainly not conclusive, it is interesting to compare its predictions to patterns of strain rate inferred from instrumentally recorded seismicity (Figure 9). After all, in southern California the instrumental seismic catalog fails to show the importance of the San Andreas fault, which is the primary plate boundary. It must be expected that the instrumental seismic catalog will be even more deficient (as a hazard assessment tool) in a place where relative velocities are an order of magnitude less.

[54] In Figure 10, we show the map pattern of long-term average, anelastic strain rates predicted by our preferred model AF-SO-013. They are strongly influenced by the map of estimated heat flows (Figure 3). A belt of high extensional strain rates running southward along the East Africa rift branches at 12°S, avoiding the strong region around the Kaapvaal craton, which *Hartnady* [2002] has named the Transgariep plate. The western branch connects to a western arc through Angola-Namibia-South Africa, and the eastern branch to a less active southeastern fan passing offshore through northern Mozambique. If this is correct, seismic hazard in Namibia is greater than that suggested by the instrumental catalog (Figure 9). On the other hand, the prominent SW-NE belt of instrumental seismicity coincident with the country of South Africa is also a feature of the model predictions, where NE-SW directed extension is predicted to occur at about 1×10^{-16} s^{-1}. This suggests that the earthquakes so clearly associated (temporally and spatially) with deep mining may be fundamentally natural tectonic earthquakes that have, however, been triggered or accelerated by human intervention.

[55] An important point is that the overall match of the strain rate field from model AF-SO-013 (Figure 10) with the instrumental seismicity (Figure 9) is rather good. This is another reason that we consider it the preferred model, even though simple model AF-SO-015 (with no lateral heterogeneities) had better predictions of stress according to some measures. Our match of the strain rate pattern is a simple result of combining correct (or approximately correct) boundary conditions with a lithosphere that contains lateral heterogeneities estimated from elevation and heat flow data. Weak fault elements played only a minor role in controlling the strain rate pattern of this model. However, if weak faults exist, their discovery, characterization, and inclusion in future models should lead to even better results.

[56] In fact, we wish to point out some deficiencies of even our preferred model that indicate the need for additional data collection and modeling in the future. First, the ENE-WSW trending Tshipise-Bosbokpoort fault system described by *Brandl* [1995] is inconsistent with the preferred model regardless of its (uncertain) sense of slip, because it is almost orthogonal to computed $\hat{\sigma}_{1H}$, but the predicted regimes in the area are NF and SS. This fault system is >170 km long, with a well-developed and -preserved scarp 2–10 m high. Episodes of reactivations were dated by the U-Th disequilibrium method at 101 ka (estimated magnitude ~8), 101–37.5 ka (~6.6), 37.5 ka (~7.6), and 29.3 ka (~6.6) [T. Partridge, unpublished data]. Second, the historical seismicity, late Pleistocene–Holocene thrust(?) faulting (with ENE-WSW strikes), and soil liquefaction features in the southern Kaapvaal craton (Koffiefontein-Florisbad-Bultfontein; between ~25°E/29.5°S and ~25°S) [*Andreoli et al.*, 1996] are also difficult to explain with the present models. These cases (and also some data from Figure 2 that we have been unable to fit) present a caveat that much remains to be learned about the complex history of faulting in this region, and that future generations

of models will also be required, either for understanding of the time-dependent strain history, or for confident projection of the future seismic hazard.

6. Conclusions

[57] This study is important as a first attempt to understand stresses and strain rates in the southern Africa region in the context of a unified model using realistic and laterally varying rheologies and density moments. We find that although southern Africa is surrounded by spreading ridges, most of it is not in a state of horizontal compression. Instead, it is generally in a state of horizontal extension because its high elevations lead to density moments exceeding those of spreading ridges. While the NW-SE band of NW-SE directed most compressive horizontal principal stress (the Wegener stress anomaly) is real, in many places it is actually caused by NE-SW extensional tectonic stress. This results from the resistance of unbroken lithosphere to the relative rotation of the incipient Somalia plate (which is distinct only in the North) away from the Africa plate. We tested the idea that this is a transient stress field around the tip of a propagating frictionless crack (the East Africa rift), but rejected that in favor of a more evolutionary model in which the faults of the rift have reduced friction (relative to unstrained plate interiors), but have enough residual friction to support an extensional tectonic stress field that activates slow extension across a wide protoplate boundary. Interestingly, the preferred model predicts much higher and differently oriented stresses in the stronger oceanic lithosphere offshore. There could be coast-parallel extensional tectonic stress close to the continental margin, and coast-parallel compressional tectonic stress farther offshore (assuming that no low-strength master faults have yet separated the AF and SO parts of the oceanic lithosphere). These predictions remain to be tested by future marine geologic and geophysical surveys. Improvements to the onshore portions of the model have the potential to yield valuable information on seismic hazard, but these may have to wait on improved knowledge of the heat flow map of southern Africa, as well as increased numbers of geodetic benchmarks whose velocities are sufficiently well constrained to fix the general location of the AF-SO pole.

[58] **Acknowledgments.** Research and publication were supported by the National Science Foundation under award EAR-0336950. The views and conclusions contained in this document are those of the authors and should not be interpreted as necessarily representing the official policies, either expressed or implied, of the U.S. Government. Funding for Marco Andreoli was provided by Nuclear Energy Corporation of South Africa and by the Inkaba ye Africa initiative of the South African National Research Foundation.

References

Andreoli, M. A. G., M. Doucoure, J. Van Bever Donker, D. Brandt, and N. J. B. Andersen (1996), Neotectonics of southern Africa: A review, *Africa Geosci. Rev.*, *3*(1), 1–16.

Baker, J., L. Snee, and M. Menzies (1996), A brief Oligocene period of flood volcanism in Yemen: Implications for the duration and rate of continental flood volcanism at the Afro-Arabian triple junction, *Earth Planet. Sci. Lett.*, *138*, 39–55.

Bassin, C., G. Laske, and G. Masters (2000), The current limits of resolution for surface wave tomography in North America (abstract), *Eos Trans. AGU*, *81*(48), Fall Meet. Suppl., Abstract S12A-03.

Behn, M. D., C. P. Conrad, and P. G. Silver (2004), Detection of upper mantle flow associated with the African superplume, *Earth Planet. Sci. Lett.*, *224*, 259–274.

Ben-Avraham, Z. (1995), Neotectonic activity offshore southeast Africa and its implications, *South African J. Geol.*, *98*, 202–207.

Ben-Avraham, Z., T. M. Niemi, and C. J. H. Hartnady (1994), Mid-Tertiary changes in deep ocean circulation patterns in the Natal Valley and Transkei Basin, southwest Indian Ocean, *Earth Planet. Sci. Lett.*, *121*, 639–646.

Ben-Avraham, Z., C. J. H. Hartnady, and A. P. le Roex (1995), Neotectonic activity on continental fragments in the southwest Indian Ocean: Agulhas Plateau and Mozambique Ridge, *J. Geophys. Res.*, *100*, 6199–6211.

Ben-Avraham, Z., G. Smith, M. Reshef, and E. Jungslager (2002), Gas hydrate and mud volcanoes on the southwest African continental margin off South Africa, *Geology*, *30*, 927–930.

Berhe, S., B. Desta, M. Nicoletti, and M. Teferra (1987), Geology, geochronology, and geodynamic implications of the Cenozoic magmatic province in W and SE Ethiopia, *J. Geol. Soc. London*, *144*, 213–226.

Bird, P. (1996), Computer simulations of Alaskan neotectonics, *Tectonics*, *15*, 225–236.

Bird, P. (1998), Testing hypotheses on plate driving mechanisms with global lithosphere models including topography, thermal structure, and faults, *J. Geophys. Res.*, *103*, 10,115–10,129.

Bird, P. (2003), An updated digital model of plate boundaries, *Geochem. Geophys. Geosyst.*, *4*(3), 1027, doi:10.1029/2001GC000252.

Bird, P., and Y. Y. Kagan (2004), Plate-tectonic analysis of shallow seismicity: Apparent boundary width, beta, corner magnitude, coupled lithosphere thickness, and coupling in seven tectonic settings, *Bull. Seismol. Soc. Am.*, *94*(6), 2380–2399.

Bird, P., and X. Kong (1994), Computer simulations of California tectonics confirm very low strength of major faults, *Geol. Soc. Am. Bull.*, *106*, 159–174.

Bird, P., and Y. Li (1996), Interpolation of principal stress directions by nonparametric statistics: Global maps with confidence limits, *J. Geophys. Res.*, *101*, 5435–5443.

Bird, P., and Z. Liu (1999), Global finite-element model makes a small contribution to intraplate seismic hazard estimation, *Bull. Seismol. Soc. Am.*, *89*, 1642–1647.

Bosworth, W., and C. K. Morley (1994), Structural and stratigraphic evolution of the Anza rift, Kenya, *Tectonophysics*, *236*, 93–115.

Brandl, G. (1995), Reactivation of certain faults in the Limpopo Belt during the Quaternary, in *Extended Abstracts of the Centennial Geocongress*, vol. 1, J. M. Barton and Y. E. Copperthwaite, pp. 442–444, Geol. Soc. of S. Africa, Johannesburg.

Brandt, D., M. A. G. Andreoli, and T. S. McCarthy (2003), Mesozoic fluvial deposits on a rifted continental margin near Vaalputs, Namaqualand, South Africa, *S. Afr. J. Geol.*, *106*, 11–16.

Brandt, D., M. A. G. Andreoli, and T. S. McCarthy (2005), The Late Mesozoic palaeosoils and Cenozoic fluvial deposits at Vaalputs, Namaqualand, South Africa: Possible depositional mechanisms and their bearing on the evolution of the continental margin, *S. Afr. J. Geol.*, *108*, 267–280.

Byerlee, J. D. (1978), Friction in rocks, *Pure Appl. Geophys.*, *116*, 615–626.

Chu, D., and R. G. Gordon (1999), Evidence for motion between Nubia and Somalia along the Southwest Indian ridge, *Nature*, *398*, 64–67.

de Wit, M. J., and I. G. D. Ransome, (1992), *Inversion Tectonics of the Cape Fold Belt, Karoo and Cretaceous Basins of Southern Africa*, 269 pp., A. A. Balkema, Brookfield, Vt.

Dingle, R. V. (1977), The anatomy of a large submarine slump on a sheared continental margin (SE Africa), *J. Geol. Soc. London*, *134*, 293–310.

Ebinger, C. J., T. Yemane, D. J. Harding, S. Tesfaye, S. Kelley, and D. Rex (2000), Rift deflection, migration and propagation: Linkage of the Ethiopian and Eastern rifts, Africa, *Geol. Soc. Am. Bull.*, *112*, 163–176.

Fernandes, R. M. S., B. A. C. Ambrosius, R. Noomen, L. Bastos, L. Combrinck, J. M. Miranda, and W. Spakman (2004), Angular velocities of Nubia and Somalia from continuous GPS data: Implications on present-day relative kinematics, *Earth Planet. Sci. Lett.*, *222*, 197–208.

Ferro, B. P. A., and D. Bouman (1987), Hydrogeological map of Mozambique, with explanatory notes, scale 1:1 000,000, Mozambique Nat. Dir. for Water Affairs, Maputo.

Fleitout, L., and C. Froidevaux (1982), Tectonics and topography for a lithosphere containing density anomalies, *Tectonics*, *1*, 21–57.

Geist, E. L., and D. J. Andrews (2000), Slip rates on San Francisco Bay area faults from anelastic deformation of the continental lithosphere, *J. Geophys. Res.*, *105*, 25,543–25,552.

Gilchrist, A. R., H. Kooi, and C. Beaumont (1994), Post-Gondwana geomorphic evolution of southwestern Africa: Implications for the controls on landscape development from observations and numerical experiments, *J. Geophys. Res.*, *99*, 12,211–12,228.

Goedhart, L. M. (2000), Field evidence for neotectonics in the south-eastern Cape, South Africa. paper presented at Neotectonics, Palaeoseismology and Seismic Hazard Analysis Workshop, Assoc. of Eng. Geol., Univ. of Stellembosch, South Africa, 23 –25 Nov.

Gordon, R. G. (1995), Present plate motions and plate boundaries, in *Global Earth Physics: A Handbook of Physical Constants*, *AGU Ref. Shelf*, vol. 1, edited by T. J. Ahrens, pp. 66–87, AGU, Washington, D. C.

Gurnis, M. (2001), Sculpting the Earth from inside out, *Sci. Am.*, *284*(3), 40–47.

Hartnady, C. J. H. (2002), Earthquake hazard in Africa: Perspectives on the Nubia-Somalia boundary, *S. Afr. J. Sci.*, *98*, 425–428.

Hatting, J., and M. L. Goedhart (1997), Neotectonic control on drainage evolution in the Algoa Basin, southeastern Cape Province, *S. Afr. J. Geol.*, *100*, 43–52.

Hill, R. S. (1988), Quaternary faulting in the south-eastern Cape Province, *S. Afr. J. Geol.*, *91*, 399–403.

Hofmann, C., V. Courtillot, G. Féraud, P. Rochette, G. Yirgu, E. Ketefo, and R. Pik (1997), Timing of the Ethiopian flood basalt event and implications for plume girth and global change, *Nature*, *389*, 838–841.

Horner-Johnson, B. C., R. G. Gordon, S. M. Cowles, and D. F. Argus (2005), The angular velocity of Nubia relative to Somalia and the location of the Nubia-Somalia-Antarctica triple junction, *Geophys. J. Int.*, *162*, 221–238.

Jackson, M. P. A., and D. K. Hobday (1980), Gravity sliding and clay diapirism in Pleistocene shoreline sequence in Zululand, South Africa, *Am. J. Sci.*, *280*, 333–362.

James, D. E., M. J. Fouch, J. C. VanDecar, S. van der Lee, and Kaapvaal Seismic Group (2001), Tectospheric structure beneath southern Africa, *Geophys. Res. Lett.*, *28*, 2485–2488.

Jimenez-Munt, I., P. Bird, and M. Fernandez (2001), Thin-shell modeling of neotectonics in the Azores-Gibraltar region, *Geophys. Res. Lett.*, *28*, 1083–1086.

Kirby, S. H. (1983), Rheology of the lithosphere, *Rev. Geophys.*, *21*, 1458–1487.

Kirby, S. H. (1985), Rock mechanics observations pertinent to the rheology of the continental lithosphere and the localization of strain along shear zones, *Tectonophysics*, *119*(1–4), 1–27.

Klein, J. A. (1980), Pleistocene to Recent faulting in the area west of Omaruru (SWA/Namibia), *Reg. Geol. Ser. Open File Rep. RG-4*, 28 pp., Geol. Surv. of Namibia, Windhoek.

Kong, X., and P. Bird (1995), Shells: A thin-plate program for modeling neotectonics of regional or global lithosphere with faults, *J. Geophys. Res.*, *100*, 22,129–22,131.

Kong, X., and P. Bird (1996), Neotectonics of Asia: Thin-shell finite-element models with faults, in *The Tectonic Evolution of Asia*, edited by A. Yin and T. M. Harrison, pp. 18–34, Cambridge Univ. Press, New York.

Lemaux, J., II, R. G. Gordon, and J.-Y. Royer (2002), Location of Nubia-Somalia boundary along the Southwest Indian ridge, *Geology*, *30*, 339–342.

Liu, Z., and P. Bird (2002a), Finite element modeling of neotectonics in New Zealand, *J. Geophys. Res.*, *107*(B12), 2328, doi:10.1029/2001JB001075.

Liu, Z., and P. Bird (2002b), North America plate is driven westward by lower mantle flow, *Geophys. Res. Lett.*, *29*(24), 2164, doi:10.1029/2002GL016002.

Marsh, J. S., R. S. Swart, and D. Phillips (2004), Implications of a new $^{40}Ar/^{39}Ar$ age for a basal flow interbedded with the Etjo Formation, northeast Namibia, *S. Afr. J. Geol.*, *106*, 281–286.

McCarthy, T. S., N. D. Smith, W. N. Ellery, and T. Gumbricht (2002), The Okavango delta: Semiarid alluvial-fan sedimentation related to incipient rifting, in Sedimentation in Continental Rifts, *Spec. Publ. SEPM Soc. Sediment. Geol.*, *73*, 179–193.

Morley, C. K., W. A. Wescott, D. M. Stone, R. M. Harper, S. T. Wigger, and F. M. Karanja (1992), Tectonic evolution of the northern Kenya rift, *J. Geol. Soc. London*, *149*, 333–348.

Mueller, D., W. R. Roest, J.-Y. Royer, L. M. Gahagan, and J. G. Sclater (1997), Digital isochrons of the world's ocean floor, *J. Geophys. Res.*, *102*, 3211–3214.

Negredo, A. M., P. Bird, C. Sanz de Galdeano, and E. Buforn (2002), Neotectonic modeling of the Ibero-Maghrebian region, *J. Geophys. Res.*, *107*(B11), 2292, doi:10.1029/2001JB000743.

Ni, S., and D. V. Helmberger (2003a), Ridge-like lower mantle structure beneath South Africa, *J. Geophys. Res.*, *108*(B2), 2094, doi:10.1029/2001JB001545.

Ni, S., and D. V. Helmberger (2003b), Seismological constraints on the South African superplume: Could be the oldest distinct structure on Earth, *Earth Planet. Sci. Lett.*, *206*(1–2), 119–131.

Ni, S., E. Tan, M. Gurnis, and D. Helmberger (2002), Sharp sides to the African superplume, *Science*, *296*, 1850–1852.

Ni, S., D. V. Helmberger, and J. Tromp (2005), Three-dimensional structure of the African superplume from waveform modeling, *Geophys. J. Int.*, *161*, 283–294.

Niu, F., A. Levander, C. M. Cooper, C.-T. A. Lee, A. Lenardic, and D. E. James (2004), Seismic constraints on the depth and composition of the mantle keep beneath the Kaapvaal craton, *Earth Planet. Sci. Lett.*, *224*, 337–346.

NOAA (1988), Digital relief of the Earth, Data Announcement, 88–MGG-02 [CD-ROM], Natl. Geophys. Data Cent., Boulder, Colo.

Partridge, T. C., and R. R. Maude (2000), Macro-scale geomorphic evolution of southern Africa, in *The Cenozoic of Southern Africa*, *Oxford Monogr. Geol. Geophys.*, vol. 40, edited by T. C. Partridge and R. R. Maude, pp. 3–18, Oxford Univ. Press, New York.

Pollack, H. N., S. J. Hurter, and J. R. Johnson (1993), Heat flow from the Earth's interior: Analysis of the global data set, *Rev. Geophys.*, *31*, 267–280.

Raab, M., R. W. Brown, K. Gallagher, A. Carter, and K. Weber (2002), Late Cretaceous reactivation of major crustal shear zones in northern Namibia: Constraints from apatite fission track analysis, *Tectonophysics*, *349*, 75–92.

Reinecker, J., O. Heidbach, M. Tingay, P. Connolly, and B. Müller (2004), The 2004 release of the World Stress Map, World Stress Map Proj. (Available online at www.world-stress-map.org)

Reznikov, M., Z. Ben-Avraham, C. Hartnady, and T. Niemi (2005), Structure of the Transkei Basin and Natal Valley, Southwest Indian Ocean, from seismic reflection and potential field data, *Tectonophysics*, *397*, 127–141.

Ritsema, J., H. J. van Heist, and J. H. Woodhouse (1999), Complex shear wave velocity structured imaged beneath Africa and Iceland, *Science*, *286*(5446), 1925–1928, doi:10.1126/science.286.5446.1925.

Stacey, T. R., and J. Wesseloo (1998), Final Project Report: Evaluation and upgrading of records of stress measurement data in the mining industry, *GAP 511b*, 31 pp. + appendices, Safety in Mines Res. Adv. Comm. (SIMRAC), Johannesburg.

Stein, C. A., and S. Stein (1992), A model for the global variation in oceanic depth and heat flow with lithospheric age, *Nature*, *359*, 123–129.

Turcotte, D. L., and G. Schubert (2002), *Geodynamics*, 2nd ed., Cambridge Univ. Press, New York.

Viola, G., M. Andreoli, Z. Ben-Avraham, I. Stengel, and M. Reshef (2005), Offshore mud volcanoes and onland faulting in southwestern Africa: Neotectonic implications and constraints on the regional stress field, *Earth Planet. Sci. Lett.*, *231*, 147–160.

Zoback, M. L., and M. D. Zoback (1989), Tectonic stress field of the continental United States, *Mem. Geol. Soc. Am.*, *172*, 523–539.

M. Andreoli, South African Nuclear Energy Corporation, P.O. Box 582, Pretoria 0001, South Africa.

Z. Ben-Avraham, Department of Geophysics and Planetary Sciences, Tel Aviv University, Tel Aviv 69978, Israel.

P. Bird and G. Schubert, Department of Earth and Space Sciences, University of California, 595 Charles Young Drive East, 3806 Geology Building, Los Angeles, CA 90095, USA. (pbird@ess.ucla.edu)

G. Viola, Geological Survey of Norway, N-7491 Trondheim, Norway.